Analyst

ROYAL SOCIETY OF CHEMISTRY

PAPER

View Article Online
View Journal

Cite this: DOI: 10.1039/d1an01034d

A novel DNA biosensor for the ultrasensitive detection of DNA methyltransferase activity based on a high-density "hot spot" SERS substrate and rolling circle amplification strategy

Shengjie Ge,[a,b,c] Menglin Ran,[d] Yu Mao,[a,b,c] Yue Sun,[a,b,c] Xinyu Zhou,[a,b,c] Li Li *[e] and Xiaowei Cao *[a,b,c]

Herein, we proposed a novel biosensor based on a high-density "hot spot" Au@SiO_2 array substrate and rolling circle amplification (RCA) strategy for the ultrasensitive detection of CpG methyltransferase (M.SssI) activity. In the presence of M.SssI, the RCA process can be triggered, causing the augmentation of the single-stranded DNA (ssDNA) at the tail of the double-stranded DNA (dsDNA), and the ssDNA can be hybridized with numerous DNA probes labeled with Raman reporters in the next steps. Afterwards, the resultant ssDNA can be modified to the Au@SiO_2 array substrate with the SERS enhancement factor of 7.49×10^6. The substrate was synthesized by using a monolayer SiO_2 array to pick up the Au nanoparticle (AuNP) array and finite-difference time-domain (FDTD) simulation showed its excellent SERS effect. Particularly, the developed biosensor displayed a significant sensitivity with a broad detection range covering from 0.005 to 50 U mL^{-1}, and the limits of detection (LODs) in PBS buffer and human serum were 2.37×10^{-4} U mL^{-1} and 2.51×10^{-4} U mL^{-1}, respectively. Finally, in order to verify the feasibility of its clinical application, the serum samples of healthy subjects and breast cancer, prostate cancer, gastric cancer and cervical cancer patients were analyzed, and the reliability of the results was also confirmed by western blot (WB) experiments. Taking advantage of these merits, the proposed biosensor can be a very promising alternative tool for the detection of M.SssI activity, which is of vital importance in the early detection and prevention of tumors.

Received 12th June 2021,
Accepted 30th June 2021

DOI: 10.1039/d1an01034d

rsc.li/analyst

1. Introduction

DNA modifications, which mainly influence gene development, play one of the most significant roles in multifarious biological processes and DNA methylation is the most common category.[1] DNA methylation has been already identified as a crucial factor in the regulation of gene expression.[2–4] In normal cells, DNA methylation mainly occurs in the repeat region of the satellite DNA while the promoter and exon genes of the CpG island are non-methylated. Once DNA methylation happens, it will affect the regulation of gene transcription and silence gene transcription.[5] When cancer occurs, the tumor suppressor genes are hypermethylated and the oncogenes outside the CpG islands are hypomethylated, resulting in the changing of the chromosomal structure, silence of the tumor suppressor gene and further invasion of the tumor.[6] Therefore, DNA methylation is closely associated with tumors. DNA methyltransferase (DNA MTase) is a chromatin modifying enzyme that can combine the methyl group to adenine or cytosine bases covalently from S-adenosyl-L-methionine (SAM), causing the occurrence of DNA methylation.[7–11] Due to the over-expression of DNA MTase before DNA methylation in many cancerous tissues, the timely detection of DNA MTase activity can help realize the early diagnosis of cancer.[12–14] Thus, a highly rapid and credible method for the detection of DNA MTase activity becomes a major demand.

In recent years, numerous approaches have been employed to detect DNA MTase activity such as high-performance liquid chromatography (HPLC),[15,16] radioactive labeling,[17] high performance capillary electrophoresis (HPCE),[18] colorimetry[19] and fluorescence.[20] However, HPLC is confined by high cost, complicated operation and it could only assess the extent of

[a]Institute of Translational Medicine, Medical College, Yangzhou University, Yangzhou, 225001, P. R. China. E-mail: cxw19861121@163.com
[b]Jiangsu Key Laboratory of Integrated Traditional Chinese and Western Medicine for Prevention and Treatment of Senile Diseases, Yangzhou University, Yangzhou, P. R. China
[c]Jiangsu Key Laboratory of Experimental & Translational Noncoding RNA Research, Medical College, Yangzhou University, Yangzhou, China
[d]The First Clinical College, Dalian Medical University, Dalian, P. R. China
[e]Children's Hospital of Nanjing Medical University, Nanjing, P. R. China. E-mail: lili12_1@126.com

total genomic DNA methylation. HPCE is limited because it needs a special running buffer and sample consumption is excessive. Other approaches are not quite outstanding due to cumbersome operation or low sensitivity. Surface-enhanced Raman scatting (SERS) is a powerful technique, mainly used to enhance the electric field intensity of metal surface plasmons by employing metal nanostructures when light is incident on the plasmons.[21–23] Recently, SERS has been widely used in biological analysis due to its advantages of rapid response, low sample use, unique fingerprint of target molecules and narrow spectral band.[24,25] Thus, SERS is a convenient, rapid and effective method for trace detection. For example, Wang's group fabricated a silver-nanoparticle-grafted silicon nanocone (AgNPs/SiNC) SERS platform *via* a droplet-confined electroless deposition (DCED) method on a superhydrophobic SiNC array to detect trace contaminants.[26] Zhu *et al.* introduced a sensitive SERS method to monitor intracellular GSH and GSSG concentrations. All the studies have lower limits of detection (LOD) than that of other methods, which confirmed the feasibility of SERS for trace detection.[27]

The SERS enhancement mechanism is generally classified into two types: electromagnetic enhancement mechanism (EM) and chemical enhancement mechanism (CM). The EM is mainly due to when the excitation occurs within the localized surface plasmon resonance of the substrate materials, the electric field will be amplified, resulting in a significant SERS enhancement effect.[28] The CM is mainly attributed to charge transfer (CT) complexes between the SERS substrates and the probe molecules adsorbed on the surface, inducing enhancement when the excitation wavelength is in resonance with the CT transition.[29] Based on the strong EM induced with excellent surface plasmon resonance effects, gold and silver nanomaterials have been widely studied and applied as SERS substrates.[30–33] However, SERS substrates made from pure Au nanoparticles (AuNPs) present poor reproducibility and significant sedimentation after absorbing probes due to the high density of noble metals, which limits their application in Raman detection. Meanwhile, noble metal nanomaterials are costly and disposable, which may lead to secondary pollution and a waste of resource. Recently, the fabrication of semiconductor/noble-metal substrates has gained attention among researchers due to the combined effects of the EM and CM.[34–37] As a new type of SERS substrate, the AuNPs@SiO_2 microsphere (Au@SiO_2) array substrate is composed of a single-layer SiO_2 array and AuNP array, and has the advantages of low cost, simple preparation, and high biocompatibility. There are two forms of electric field enhancement on the substrate: one is distributed in the gap between adjacent Au nanoparticles, and the other is located in the "V" shaped area at the junction of adjacent SiO_2 microspheres. This structure provides effective sites for the loading of the single-layer AuNP array, and the combination of two ordered arrays realizes the uniform distribution of high-density "hot spots", resulting in an excellent SERS performance. As a result, the Au@SiO_2 substrate is a potential candidate for SERS detection.

In the last few years, SERS-based detection of DNA MTase activity has gained a lot of attention due to its great enhancement effect.[38–40] However, for some low concentration targets, the SERS method still cannot meet the requirements of ultrasensitive detection, so it is quite necessary to introduce a signal amplification strategy. Previously, multiple isothermal amplification strategies have been introduced to enhance the detection sensitivity, such as nicking enzyme signal amplification (NESA),[41] strand displacement amplification (SDA)[42] and rolling circle amplification (RCA). SDA is limited due to its high noise signal and the detection sensitivity may be affected by its linear amplification. The NESA-based method requires harsh conditions such as denaturing the molecular beacon by initial heating and a specific oligonucleotide. Among these, RCA has attracted research attention for its advantages of simplicity, excellent efficiency, versatility and low background noise. Moreover, another outstanding advantage of the RCA technique is that its product can be fixed on a solid substrate because of its great compatibility and this preponderance made it possible to detect DNA MTase activity *via* SERS combined with the RCA double enhancement strategy.[43]

In this paper, a neoteric biosensor based on the Au@SiO_2 array substrate and RCA strategy was designed for the ultrasensitive detection of M.SssI activity, a CpG MTase. During the preparation of the Au@SiO_2 array substrate, the Langmuir-Blodgett (L-B)[44] method was used to obtain a single-layer SiO_2 array, then the AuNP array covering on the surface of the SiO_2 array was synthesized *via* the oil–water interface self-assembly method. Finite-difference time-domain (FDTD) simulations were used to evaluate the electromagnetic field enhancement. In the RCA process, the single-stranded DNA (ssDNA) at the tail of the double-stranded DNA (dsDNA) can be amplified under the function of padlock DNA and DNA polymerase (Phi29) in the presence of M.SssI. The ssDNA sequences were linked to the surface of the Au@SiO_2 array substrate after hybridizing with numerous short DNA signal probes labeled with Raman reporters (5-FAM). The uniformity, reproducibility and stability were assessed to confirm the performance of this design. The experimental conditions were optimized for the fabrication of a highly sensitive biosensor, including the catalytic time of M.SssI, cutting time of HpaII, reaction time of RCA and hybridization time of the DNA signal probe. In order to evaluate the sensitivity of this biosensor, SERS was applied to analyze the M.SssI activity simultaneously in phosphate-buffered saline (PBS) and human serum based on a high-density "hot spot" Au@SiO_2 array substrate and RCA strategy. Finally, the M.SssI activity in human serum of several kinds of cancer patients such as breast cancer patients, prostate cancer patients, gastric cancer patients and cervical cancer patients was detected by SERS, proving the potential of the SERS-based biosensor for the early diagnosis of cancer.

2. Materials and methods

2.1 Chemicals

Ethyl orthosilicate ($C_8H_{20}O_4Si$), absolute ethanol, chloroauric acid tetrahydrate ($HAuCl_4$), methanol, sodium dodecyl sulfate

(SDS), magnesium chloride ($MgCl_2$), magnesium acetate ($Mg(Ac)_2$), hydrogen peroxide (H_2O_2), sulfuric acid (H_2SO_4), ammonium hydroxide (NH_4OH), tris hydrochloride (Tris-HCl), dithiothreitol (DTT), bovine albumin (BSA), sodium chloride (NaCl) and potassium Acetate (KAc) were obtained from Sigma-Aldrich Chemical Co. Ltd (Shanghai, China). Trisodium citrate dihydrate ($Na_3C_6H_5Na_3O_7{\cdot}2H_2O$), hexane ($C_6H_{14}$), chloroform ($CHCl_3$) and silicon wafers were all provided by Younuo Chemicals Co. Ltd (Yangzhou, China). All the ultra-pure water used was produced by a Milli-Q purifier (Millipore, USA, resistivity >18 M). As is shown in Table 1, primer 1, primer 2, padlock DNA and 5-carboxyfluorescein (5-FAM) probe were purchased from Sangon Biotech Co. Ltd (Shanghai, China). T4 DNA polymerase, CpG methyltransferase (M.SssI), restriction endonuclease Msp I (HpaII), Phi29 DNA polymerase and S-adenosyl-L-methionine (SAM) were provided by Linc-Bio Science Co. Ltd (Shanghai, China). All the beakers used were immersed in newly prepared aqua regia solution and then rinsed thoroughly with ultra-pure water, followed by drying.

2.2 Preparation of the Au@SiO_2 array substrate

2.2.1 Synthesis of the SiO_2 array. Silicon samples with a size of 10 mm × 15 mm were all exhaustively cleaned three times with ultra-pure water and absolute ethanol. Then, the silicon wafers were immersed in piranha solution for 30 min followed by drying, and the piranha solution was prepared by mixing hydrogen peroxide (30 wt%) with concentrated sulfuric acid in a ratio of 3 : 7 by volume. The sol-gel method was adopted to synthesize SiO_2.[45] Firstly, 20 mL of NH_4OH and 100 mL of ethanol were mixed with 12 mL of ultra-pure water in a breaker and heated to 30 °C. It can be found that the color of the mixed solution became milky white after adding 20 mL of $C_8H_{20}O_4Si$ drop by drop. SiO_2 could be obtained after reacting for 12 h. In the end, SiO_2 was dispersed in methanol solution after being subjected to centrifugation (4000 rpm, 15 min), thus a suspension of SiO_2 with a concentration of 5 wt% could be obtained. The Langmuir-Blodgett (LB) gas-liquid interface assembly method was adopted to manufacture the SiO_2 array. Firstly, $CHCl_3$ was mixed with the prepared SiO_2 suspension in a ratio of 2 : 3 by volume. Then, 5 μL of the mixed solution was measured each time and dropped onto the water surface until the SiO_2 covered the entire surface spontaneously. Subsequently, after dropping 100 μL of SDS aqueous solution (2 wt%) onto the water surface, the formation of a tightly aligned single-layer SiO_2 array could be observed. Finally, the single-layer SiO_2 array was transferred to a prepared hydrophilic silicon wafer followed by drying. The air plasma cleaning machine was used to improve the hydrophilicity of the SiO_2 array.

2.2.2 Preparation of the Au@SiO_2 array substrate. AuNPs were prepared according to Khezri's method.[46] The Au@SiO_2 array substrate was fabricated *via* the oil-water interface self-assembly method. Briefly, 8 mL of the prepared AuNP colloidal solution was mixed with 4 mL of hexane in a beaker sequentially and then it could be found that AuNPs formed a neat array at the oil-water interface after adding 4 mL of ethanol drop by drop. Next, the prepared monolayer SiO_2 array was used to pick up the AuNP array followed by drying. Thus, the Au@SiO_2 array substrate could be obtained.

2.3 Methylation and cleavage of dsDNA

Firstly, 1 μL of dsDNA solution (2 mM), 15 μL of 1× NEB buffer (50 mM NaCl, 10 mM Tris-HCl, 10 mM $MgCl_2$ and 1 mM DTT), 1.5 μL of SAM, ultra-pure water and different concentrations of M.SssI (0, 0.005, 0.01, 0.1, 1, 5, 10, 50 U mL^{-1}) were added to a centrifuge tube and reacted for 2 h. Then, 20 μL of 1× Cut Smart buffer (50 mM KAc, 20 mM Tris, 10 mM $Mg(Ac)_2$ and 100 mg BSA), 3 mL of ultra-pure water and 1 mL of HpaII solution were mixed with an active concentration of 5 U μL^{-1} for 1 h. Thus, the unmethylated dsDNA in the reaction solution has been cut. Later on, 20 μL of 1× Phi29 DNA buffer, 200 mM free bases (A, T, C, G) and 4 U mL^{-1} Phi29 DNA polymerase were added to the mixture. After 30 min, the ssDNA was amplified into a long DNA strand along the circular template. Finally, the DNA product clean-up kit was employed for the recycling and purification of the RCA reaction products. Meanwhile, agarose (3 wt%) gel electrophoresis was performed on the products after three stages of the reaction.

2.4 Detection of M.SssI activity

First of all, purified RCA reaction products, PBS buffer and 40 μL of ultra-pure water were mixed to obtain 50 μL of RCA reaction product assembly buffer. Then, the as-prepared Au@SiO_2 array substrate was immersed into the solution and it was ensured that the substrate was submerged in the solution completely. Next, the centrifuge tube was incubated in a constant temperature mixer for 16 h. Later on, the substrate was immersed in the prepared DNA signal probe solution and incubated for another 24 h. Finally, the substrate was flushed with ultra-pure water to remove excess signal probe, then SERS measurements were performed.

2.5 Characterization

The S-4800 II field emission scanning electron microscope (Hitachi, Japan) was used to characterize the morphology of nanomaterials. The Raman experiments were carried out at

Table 1 Name and sequence of DNA used in the MTase activity test

Name	Sequence
Primer 1	SH-$(CH_2)_6$-TTCTCTTCCTCTGTGCGCCGGTCGCTCCCAGGCATTAATGCTAATCGTGATAGGGGT
Primer 2	CCTGGGAGAGACCGGCGCACAGAGGAAGAGAA
Padlock DNA	PO_4-CGATTAGCATTCAGAATCATGATAGCGCGCAACGGGCCTGGGTGGTGGGGAAGCGCGCTATCA
DNA signal probe (5-FAM probe)	GAAAGCGATCTATAATCCCTACACCAC-5FAM

785 nm with a 50× long working distance objective by using a Renishaw InVia micro-Raman microscope. The laser power and acquisition time were set as 5 mW and 10 s, respectively. For the characterization of the substrate, 4-MBA with a concentration of 1×10^{-4} M was selected as the signal molecule.

2.6 Ethics statement

The peripheral blood specimens were obtained from 150 volunteers provided by the Affiliated Hospital of Yangzhou University including 30 breast cancer patients, 30 prostate cancer patients, 30 gastric cancer patients, 30 cervical cancer patients and 30 healthy subjects. Details about the gender and age are summarized in Table 2. The whole experiments were performed in accordance with the Guidelines "Declaration of Helsinki", and approved by the ethics committee at Yangzhou University. Informed consent was obtained from the human participants of this study.

Table 2 Characteristics of the research subjects

Group	Healthy	Breast cancer	Prostate cancer	Gastric cancer	Cervical cancer
Gender					
Male	17	15	30	18	14
Female	13	15	0	12	16
Average age	29	46	55	53	50
Sample	30	30	30	30	30

3. Results and discussion

3.1 Principle of the Au@SiO_2 array substrate and RCA strategy

As shown in Scheme 1A, the SiO_2 array was prepared *via* the LB gas-liquid interface assembly method and SDS was used as a surfactant to arrange it in a single layer. Using the prepared SiO_2 array to pick up the AuNP array synthesized by the oil-water interface self-assembly, the Au@SiO_2 array substrate could be obtained (Scheme 1B). There are three recognition sites on the dsDNA (synthesized by Primer 1 and Primer 2) in the RCA system: one is for the DNA MTase (M.SssI); one is for the methylation sensitive restriction endonuclease (HpaII) and another site is for the circular template required for the RCA reaction (Padlock DNA). As presented in Scheme 1C, the DNA MTase recognition site on the dsDNA can be recognized in the presence of M.SssI, and the unmethylated dsDNA (5′-CCGG-3′) could be catalyzed to methylated dsDNA (5′-CCmGG-3′) (changed from purple to light blue). HpaII is an endonuclease that can cut the unmethylated dsDNA, thus the dsDNA catalyzed by M.SssI could not be cut. Furthermore, the ssDNA at the tail of dsDNA was bound to the padlock DNA to further trigger the RCA process. Then DNA polymerase (Phi29) and

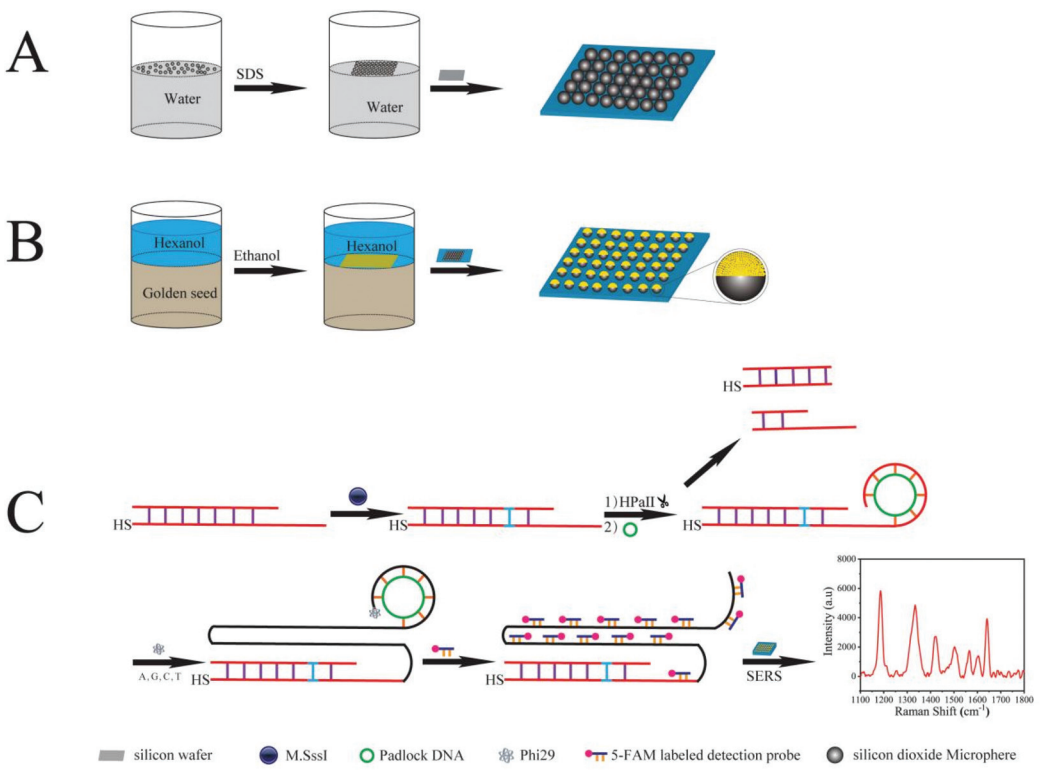

Scheme 1 Schematic diagram of the biosensor combined with the RCA strategy for analyzing the M.SssI activity sensitively. (A) The synthesis process of a single-layer SiO_2 array. (B) The preparation of the Au@SiO_2 array substrate. (C) RCA process and SERS detection in the presence of M. SssI.

four free bases were added, and the ssDNA expanded continuously along the circular template into a long single strand composed of a series of repeated sequences (black strand). The amplified ssDNA could be hybridized with numerous DNA probes labeled with 5-FAM and then it could be fixed to the as-prepared Au@SiO_2 array substrate using the thiol group, thus the amplification of SERS signals could be realized. In contrast, the unmethylated dsDNA was cleaved into two fragments under the function of HpaII and could not trigger the RCA process. Thus, the biosensor based on the Au@SiO_2 array substrate and RCA strategy can be used for the detection of M.SssI activity.

3.2 Characterization of Au@SiO_2 array substrates

The preparation of a single-layer SiO_2 array is presented in Scheme 1. As a surfactant, SDS plays an important role in the formation of a single-layer SiO_2 array. On the one hand, SDS can guide the as-prepared SiO_2 microspheres to form a certain degree of aggregation. On the other hand, SDS plays the role of a glue which allowed the single SiO_2 microspheres to connect with each other and form an orderly array substrate instead of excessive accumulation. Therefore, under the function of SDS, the more the SiO_2 microspheres are generated, the denser the array will be. As shown in Scheme 1, the charge density of AuNP surface was reduced due to the addition of ethanol, realizing the self-assembly of AuNPs at the oil-water interface to form a monolayer of the AuNP array as shown in Fig. 1A and the inset. It could be observed that the AuNP array tiled neatly at the oil-water interface, the distribution of AuNPs is relatively uniform and the diameter is about 20 nm. The SEM image of the SiO_2 array is shown in Fig. 1B and it could be indicated that the opal structure was composed of a single-layer SiO_2 array which arranged orderly on the hydrophilic silicon wafer with an average size of about 450 nm. Fig. 1C and D present the SEM images of the Au@SiO_2 array substrate at different magnifications and it could be found that the AuNPs spread on the surface of the SiO_2 array closely and orderly. In order to test the various properties of the substrate, 4-MBA (1×10^{-4} M) was modified on the surface of the Au@SiO_2 array substrate (4-MBA-Au@SiO_2). A SERS mapping was performed on the surface of the 4-MBA-Au@SiO_2 substrate to evaluate the uniformity of the Au@SiO_2 array substrate. The scanning range and the peak intensity were set to 50 × 50 mm^2 and 1593 cm^{-1}, respectively. The SERS characteristic peak at 1593 cm^{-1} was due to the non-totally symmetric ν(CC) mode.[47] The Raman signal intensity at 1593 cm^{-1} was represented by the change of color where blue represented the minimum signal and red represented the maximum signal. As shown in Fig. 1E, although there were some blue areas in the image, the color distribution was basically regular, indicating the high uniformity of the Au@SiO_2 array substrate and the relative standard deviation (RSD) value was calculated to be 6.9%. Furthermore, the SERS spectra of 20 random sites were obtained from the surface of the 4-MBA-Au@SiO_2 substrate as

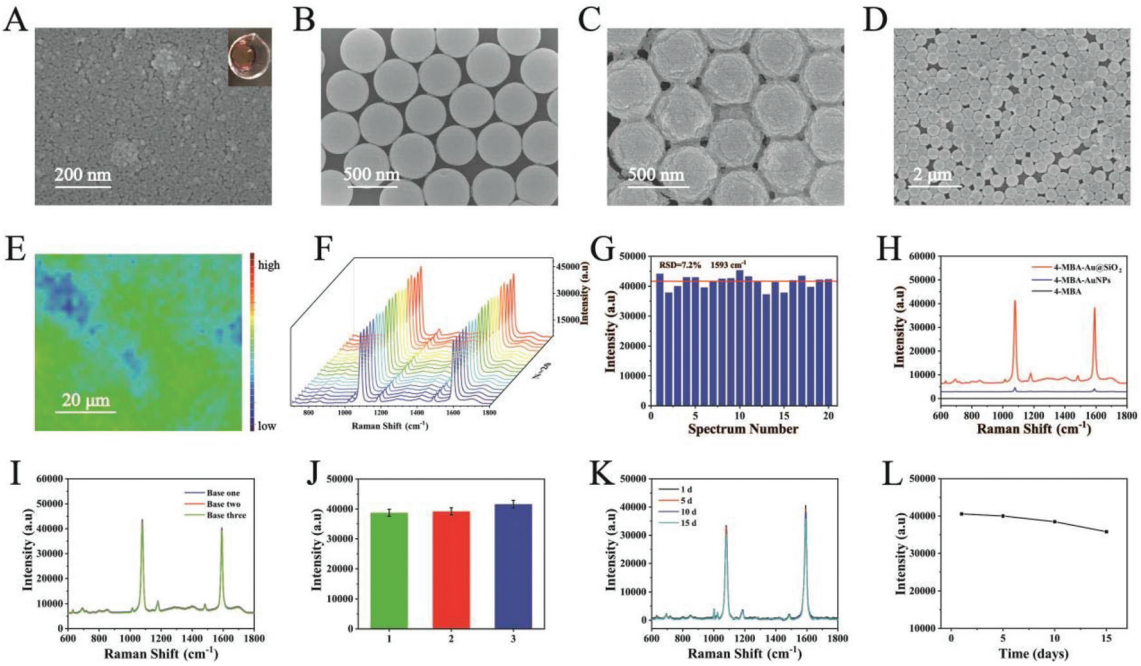

Fig. 1 SEM images of (A) the monolayer AuNP array and (B) single-layer SiO_2 array. SEM images of the Au@SiO_2 array substrate at different magnifications: (C) high magnification, (D) low magnification. (E) A SERS mapping for the 4-MBA-Au@SiO_2 substrate. (F) SERS spectra of 20 random sites selected from the 4-MBA-Au@SiO_2 substrate and (G) the bar chart of the signal intensities at 1593 cm^{-1}. (H) SERS spectra of the 4-MBA-Au@SiO_2 substrate, 4-MBA-AuNPs substrate and 4-MBA at 1593 cm^{-1}. (I) SERS spectra of three 4-MBA-Au@SiO_2 substrates synthesized at different times and (J) the bar chart of the signal intensities at 1593 cm^{-1}. (K) The average SERS spectra of the 4-MBA-Au@SiO_2 substrate after being stored for 1 d, 5 d, 10 d and 15 d at a room temperature respectively and (L) the corresponding line chart of the signal intensities at 1593 cm^{-1}.

shown in Fig. 1F and G along with the bar chart of intensities at 1593 cm^{-1} with an RSD value of 7.2%. Therefore, the Au@SiO_2 array substrate has significant uniformity. We also measured the SERS spectra of three 4-MBA-Au@SiO_2 substrates synthesized at different times. As Fig. 1I and J illustrate, the deviation of the signal intensities at 1593 cm^{-1} was 5.75%, proving that the Au@SiO_2 array substrate had great reproducibility. Fig. 1K shows the average signal intensities of the 4-MBA-Au@SiO_2 substrate after being stored for 1 d, 5 d, 10 d and 15 d at room temperature and no significant signal reduction could be found. Fig. 1L further illustrates that the total reduction of the SERS intensity at 1593 cm^{-1} after 15 d was 11.7%, proving the great stability of the Au@SiO_2 substrate. In the end, we also evaluated the SERS enhancement capability of the Au@SiO_2 array substrate as shown in Fig. 1H. The corresponding Raman enhancement factor (EF) value of the 4-MBA-Au@SiO_2 substrate and 4-MBA-AuNPs substrate at 1593 cm^{-1} was 7.49×10^6 and 3.12×10^5, calculated by referring to the equation: $EF = (I_{SERS}/C_{SERS})/(I_{Raman}/C_{Raman})$. Here I and C represent the signal intensity at 1593 cm^{-1} and the concentration of 4-MBA, respectively. Therefore, the Au@SiO_2 array substrate has a significant enhancement capability of the SERS signal compared to ordinary noble metal substrates.

3.3 FDTD simulations

In order to further study the mechanism of signal enhancement on the Au@SiO_2 array substrate under the irradiation of a beam of linearly polarized light, the FDTD simulation was performed. Fig. 2A and B show the model of the Au@SiO_2 array substrate used for the simulation from the upper and lateral views and all the geometric parameters were set according to the average value of the actual sample as shown in Fig. 1C. Fig. 2C demonstrates that the surface of the SiO_2 microspheres was covered with the enhanced electric field and "V" shaped gaps between adjacent SiO_2 microspheres showed more significant electric field enhancement than elsewhere. This could be explained by the difference of the distance between AuNPs distributed on the surface of the single-layer SiO_2 array and the distance in the gap was much smaller than that along the surface. Fig. 2D and E present the typical electric field distribution of the substrate when z = 225 nm and z = 450 nm in the x–y plane, respectively. Fig. 2D further proves that the electric field enhancement in the "V" shaped gaps was much stronger than those in other regions. As shown in Fig. 2E, the electric field on the top surface of the Au@SiO_2 array substrate still showed a significant enhancement while the LSPR effect has been weakened notably due to the augment of the distance between the AuNPs. Therefore, the Au@SiO_2 array substrate could generate significant signal enhancement because of the formation of a great deal of high-density "hot spots" even through the top surface; thus it can exhibit an excellent SERS effect.

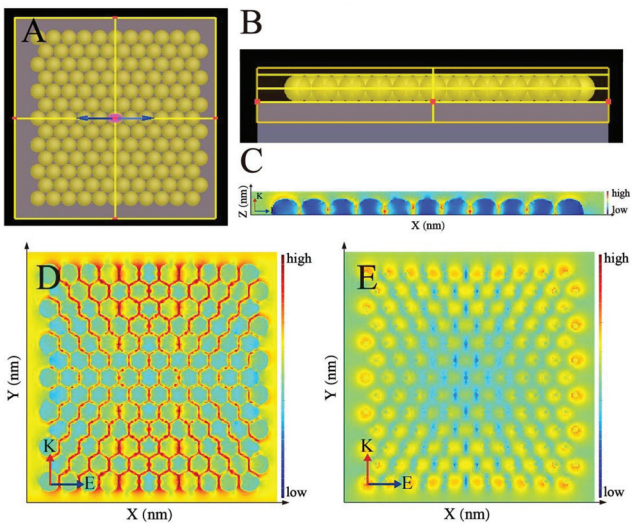

Fig. 2 (A) The upper and (B) lateral views of the Au@SiO_2 array substrate model. (C) The simulated electric field intensity distribution images of the substrate from the lateral view. The simulated electric field intensity distribution images of the substrate from the upper view when (D) z = 225 nm and (E) z = 450 nm.

3.4 Characterization of the RCA process

In order to verify the recognition effect of HpaII in the process of the RCA reaction, an agarose gel electrophoresis (AGE) analysis was performed. As shown in Fig. 3A, there was only one band at lane 1, representing a pure dsDNA (57 bp), and the appearance of a new 38 bp DNA band at lane 2, indicating that HpaII could recognize unmethylated dsDNA and cut it. However, when the dsDNA reacted with HpaII after being catalyzed by M. SssI, there was just one band at lane 3 which represented the dsDNA, indicating that no cleavage reaction occurred and HpaII could not recognize the methylated dsDNA. Fig. 3B presents the AGE analysis of the RCA reaction product in the presence of Phi29 DNA polymerase and it demonstrates that the RCA reaction was successfully triggered by Phi29 DNA polymerase to produce a new DNA band with a larger molecular weight and the dsDNA could not grow along the circular template if no Phi29 DNA polymerase existed. The above phenomena indicated that HpaII could effectively recognize and catalyze the unmethylated dsDNA, and Phi29 DNA polymerase can further trigger the occurrence of the RCA reaction. As is shown in Fig. 3C, line two and line one represented the Raman spectra before and after the RCA process, respectively. It could be used to demonstrate that the dsDNA has been amplified to a great extent which caused the significant enhancement of the Raman signal.

3.5 Optimization of experimental conditions

The biosensor developed in this work mainly relied on the RCA strategy. Therefore, optimizing the experimental conditions including the catalytic time of M.SssI, cutting time of HpaII, reaction time of RCA and hybridization time of the DNA signal probe could be beneficial to obtain the best analysis and detection performance. The SERS characteristic peaks of 5-FAM at 1640 cm^{-1} and 1344 cm^{-1} were due to the xanthene ring vibrations and the peak at 1498 cm^{-1} was due to

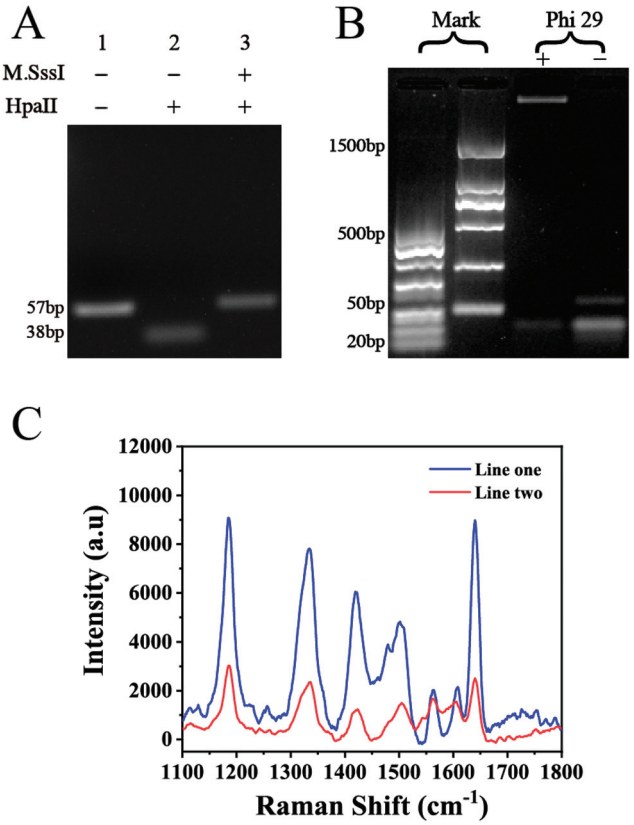

Fig. 3 (A) AGE analysis of DNA products catalyzed by M.SssI and HpaII. The three lanes represented pure dsDNA, the product of dsDNA catalyzed by HpaII and the product of dsDNA catalyzed by HpaII after being catalyzed by M.SssI, respectively. (B) AGE analysis of the RCA reaction product in the presence of Phi29 DNA polymerase after binding to the circular template. (C) Raman spectra of 5-FAM before and after the RCA process.

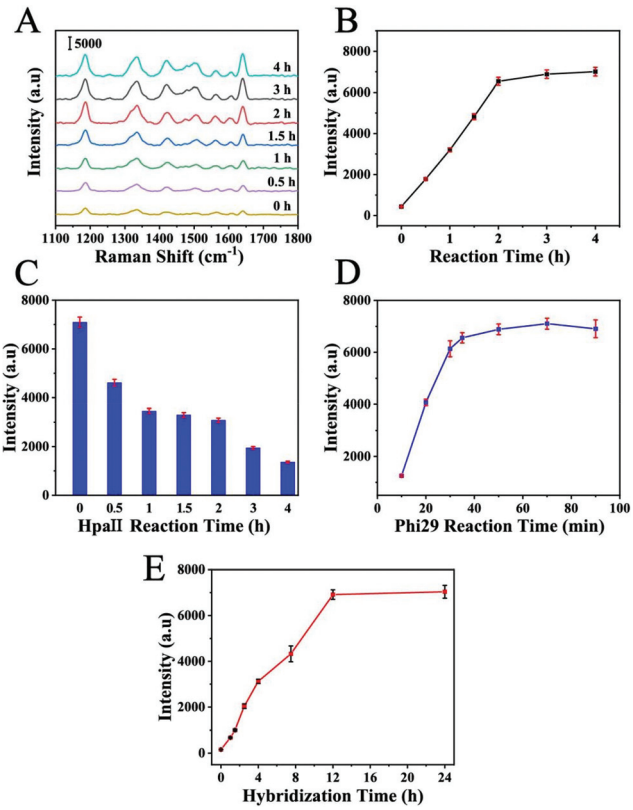

Fig. 4 (A) SERS spectra of 5-FAM in the presence of M.SssI with the same activity and different incubation times (0, 0.5, 1, 1.5, 2, 3 and 4 h). (B) Corresponding line chart of the signal intensities at 1334 cm^{-1}. (C) Bar chart of the signal intensities at 1334 cm^{-1} against different reaction times of HpaII. Line chart of the signal intensities at 1334 cm^{-1} against the reaction time of (D) RCA and (E) hybridization time.

a central ring breathing vibration.[48] M.SssI with the same active concentration was used to evaluate the influence of the catalytic time on the determination of DNA MTase activity by changing the catalytic time to 0 h, 0.5 h, 1 h, 1.5 h, 2 h, 3 h and 4 h respectively. As shown in Fig. 4A and B, Raman intensities at 1334 cm^{-1} increased with the extension of catalytic time and the growth trend slowed markedly when the catalytic time increased to 2 h. Then, no further significant increase was observed with the further extension of catalytic time indicating the stability of the DNA methylation reaction, thus 2 h was the best catalytic time for DNA methylation. The cutting time of HpaII was equally important for experiments and the final result will be higher than the real value if the reaction time is too short. Fig. 4C presents the signal intensities at 1334 cm^{-1} along with the extension of the cutting time of HpaII, indicating that Raman intensities decreased gradually with the time ranging from 0 h to 4 h and the intensities had changed weakly since the reaction time increased to 1 h caused by the completion of most DNA cutting. Thus, the optimal cutting time of HpaII should be adjusted to 1 h. Finally, we also adjusted the reaction time of RCA and the hybridization time of the DNA signal probe to 30 min and 12 h as shown in Fig. 4D and E, respectively.

3.6 Detection of M.SssI activity

The sensitivity of the biosensor was evaluated under the optimized conditions. M.SssI was added to PBS and human serum and was diluted to different concentrations followed by SERS detection. Fig. 5A presents the SERS spectra of 5-FAM in the presence of different concentrations of M.SssI *via* the biosensor in PBS buffer. It could be illustrated that the signal intensities decreased along with the decrease of M.SssI concentrations. Particularly, as shown in Fig. 5B, there was a great linear relationship between the signal intensity at 1334 cm^{-1} and the logarithmic concentration of M.SssI. The corresponding linear equation is $y = 1610.84x + 4948.18$ and the correlation coefficient (R^2) is 0.9934. The limit of detection (LOD) was calculated to be 2.37×10^{-4} U mL^{-1}. In order to further study the sensitivity in human serum, the SERS spectra were obtained as shown in Fig. 5C. The results demonstrated that the SERS spectra analyzed in human serum were fairly close to those analyzed in PBS buffer, proving that the biosensor still showed great accuracy in human serum. There was still a great

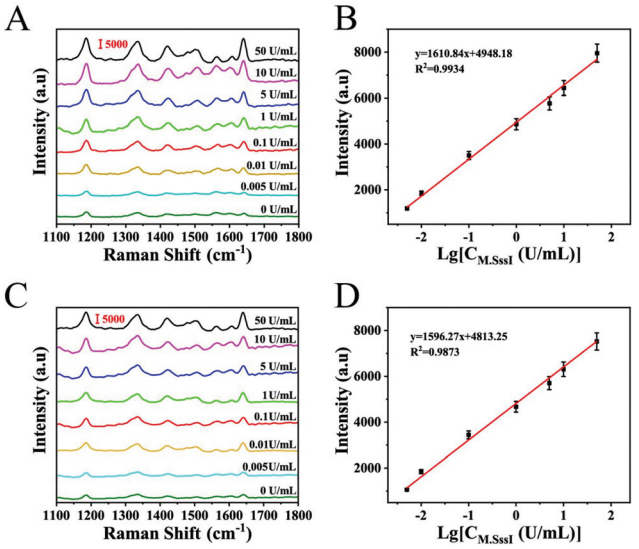

Fig. 5 SERS spectra of 5-FAM in the presence of M.SssI in (A) PBS buffer and (C) human serum with different concentrations (0, 0.005, 0.01, 0.1, 1, 5, 10 and 50 U mL^{-1}). Corresponding calibration curve of SERS intensities at 1334 cm^{-1} in (B) PBS buffer and (D) human serum.

linear relationship between the signal intensity at 1334 cm^{-1} as shown in Fig. 5D and the logarithmic concentration of M. SssI and the linear regression equation is $y = 1596.27x + 4813.25$, $R^2 = 0.9873$. The LOD was calculated to be 2.51×10^{-4} U mL^{-1}. Then the sensitivity of the biosensor proposed in this work was compared to those of other reported methods as shown in Table 3. The result demonstrated that the LOD in this work was much lower than that of many reported methods. Therefore, the biosensor has great application prospects in the detection of M.SssI activity.

3.7 Selectivity of the biosensor

In order to evaluate the selectivity of the biosensor based on the proposed strategy, another DNA MTase (DNA adenine MTase, DAM) was introduced as an interference option. The constructed biosensor was used for the detection of three groups of samples: the first group was a control group containing no DNA MTase, the second group was M.SssI at a concentration of 50 U mL^{-1} and the last group contained Dam with a concentration of 50 U mL^{-1}. Fig. 6A presents the SERS spectra of 5-FAM finally detected with the three groups of samples. The

Table 3 Comparison of the proposed biosensor with the reported methods for M.SssI detection

Methods	Linear range (U mL^{-1})	Detection limit (U mL^{-1})	Ref.
Colorimetry	0.2–50	0.08	49
Fluorescence	0.5–80	0.019	50
Fluorescence	0.1–4	0.06	51
Electrochemistry	0.25–10	0.18	52
SERS	0.05–50	2.8×10^{-3}	53
SERS	0.005–50	2.51×10^{-4}	This work

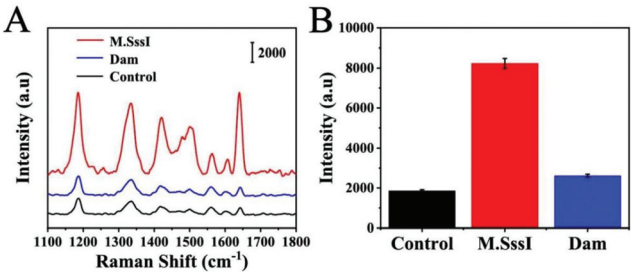

Fig. 6 (A) SERS spectra of 5-FAM in the presence of M.SssI (50 U mL^{-1}), DAM (50 U mL^{-1}) and the control group. (B) Corresponding bar chart of the intensities at 1334 cm^{-1}.

result demonstrated that only the M.SssI group could detect significant SERS spectra of 5-FAM, while the signal of the interference group was extremely weak and its intensity at 1334 cm^{-1} was similar to that of the control group (Fig. 6B). These data showed that the constructed biosensor had a specific response to M.SssI samples, which proved that the biosensor has outstanding selectivity. Therefore, the proposed biosensor could be applied to detect M.SssI activity characteristically.

3.8 Clinical serum sample analysis

To demonstrate the application prospect and accuracy of the proposed biosensor in clinical serum samples, we also

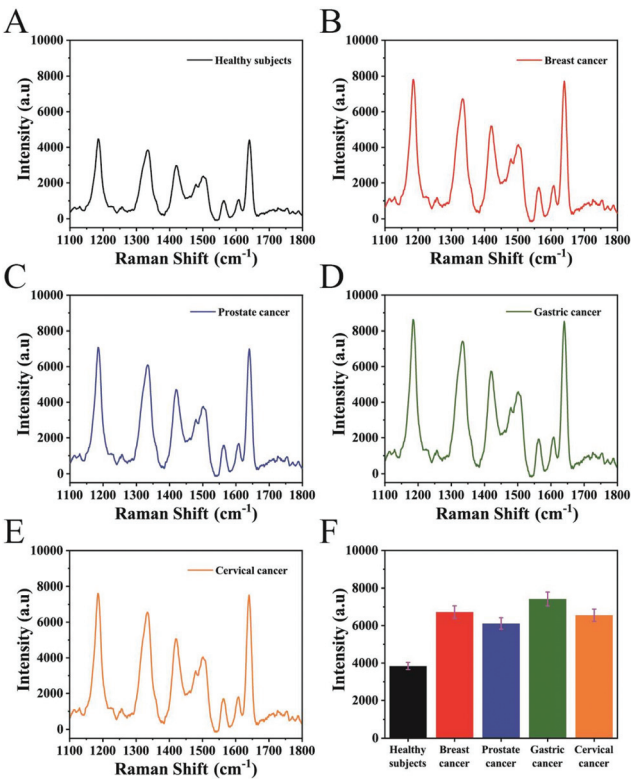

Fig. 7 Average SERS spectra of the clinical serum samples obtained from (A) healthy subjects, (B) breast cancer patients, (C) prostate cancer patients, (D) gastric cancer patients and (E) cervical cancer patients. (F) Corresponding histogram of the peak intensities at 1334 cm^{-1}.

Table 4 Mean levels of M.SssI activity in clinical serum samples

Method	Healthy	Breast cancer	Prostate cancer	Gastric cancer	Cervical cancer
SERS (U mL^{-1})	0.247 ± 0.021	15.717 ± 0.064	6.509 ± 0.024	43.067 ± 0.079	12.325 ± 0.044
WB (U mL^{-1})	0.239 ± 0.012	16.316 ± 0.031	6.783 ± 0.042	41.164 ± 0.027	11.734 ± 0.053
Relative error (%)	3.35	−3.67	−4.04	4.62	5.04

detected the M.SssI activity in the collected 150 serum samples (30 breast cancer patients, 30 prostate cancer patients, 30 gastric cancer patients, 30 cervical cancer patients and 30 healthy subjects) and their average SERS spectra are shown in Fig. 7B, C, D, E, and A. The corresponding bar chart of the signal intensities at 1334 cm^{-1} is shown in Fig. 7F. It could be observed that the M.SssI activity in the serum samples of healthy subjects was much lower than that in cancer patients, further evidencing that M.SssI activity was associated with the development of cancer closely. Moreover, a comparison between SERS detection results and the results obtained by WB is shown in Table 4. The results of the comparison further proved the reliability of the proposed biosensor for the detection of M.SssI activity and it could be used for the early screening of a variety of cancers.

4. Conclusions

In conclusion, a novel biosensor based on the Au@SiO_2 array substrate and RCA strategy was developed to detect M.SssI activity in human serum by measuring the SERS intensities of 5-FAM. The proposed substrate could form a great deal of high-density "hot spots" even on its top surface, which can cause significant SERS signal enhancement. Meanwhile, the biosensor showed a wide linear response ranging from 0.005 to 50 U mL^{-1} whether in PBS or human serum, and the LODs were as low as 2.37×10^{-4} U mL^{-1} and 2.51×10^{-4} U mL^{-1}, respectively. In addition, this biosensor showed the advantages of great uniformity, reproducibility, stability and sensitivity, compared to other methods. This biosensor has successfully detected M.SssI activity in human serum of several kinds of cancer patients such as breast cancer patients, prostate cancer patients, gastric cancer patients and cervical cancer patients. This work provides a rapid and ultrasensitive method for the detection of M.SssI which could be favourable for the screening of anticancer drugs, showing great application prospect in the future.

Author contributions

Shengjie Ge: conceptualization, methodology, validation, investigation, resources and writing-original draft preparation; Menglin Ran: formal analysis; Yu Mao: data curation; Yue Sun: visualization; Xinyu Zhou: software and supervision; Li Li: writing-review and editing, project administration and funding acquisition; Xiaowei Cao: writing-review and editing, project administration and funding acquisition.

Conflicts of interest

There are no conflicts to declare.

Acknowledgements

This research was funded by the National Natural Science Foundation of China (No. 81701825), the Social Development Foundation of Jiangsu (No. BE2018684) and the Science and Technology Development Fund of Nanjing Medical University (NMUB2018093).

References

1 L. Wang, J. Zhang, J. Duan, X. Gao, W. Zhu, X. Lu, L. Yang, J. Zhang, G. Li, W. Ci, W. Li, Q. Zhou, N. Aluru, F. Tang, C. He, X. Huang and J. Liu, Programming and Inheritance of Parental DNA Methylomes in Mammals, *Cell*, 2014, **157**, 979–991.

2 M. Dadmehr, M. A. Karimi and B. Korouzhdehi, A signal-on fluorescence based biosensing platform for highly sensitive de-tection of DNA methyltransferase enzyme activity and inhibition, *Spectrochim. Acta, Part A*, 2020, **228**, 117731.

3 L. J. Wang, M. Afsaneh, W. L. Li, L. Jesper, S. X. Li, C. Signe, T. Maria, S. Mette, M. F. Jonas, C. Kaare, H. Jacob and Q. H. Tan, Genetic and environmental determinants of O^6-methylguanine DNA-methyltransferase (MGMT) gene methylation: a 10-year longitudinal study of Danish twins, *Clin. Epigenet.*, 2021, **13**, 35.

4 H. Q. Chen, D. J. Chen, Y. Li, F. Han, X. Jiang, J. Cao, J. Y. Liu and W. B. Liu, DNA methylation and hydroxymethylation as-sociated with gene expression regulatory network during 3-methylcholanthrene induced lung cell malignant transfor-mation, *Sci. Total Environ.*, 2021, **771**, 144839.

5 H. H. Tang and B. E. Gold, Homo sapiens Lactate Dehydrogenase c (Ldhc) gene expression in cancer cells is regulated by transcription factor Sp1, CREB and CpG Island Methylation, *Andrology*, 2009, **30**, 157–167.

6 M. Esteller, P. G. Corn, S. B. Baylin and J. G. Herman, A gene hypermethylation profile of human cancer, *Cancer Res.*, 2001, **61**, 3225–3229.

7 D. Smith and A. Meissner, DNA methylation: roles in mammalian development, *Nat. Rev. Genet.*, 2013, **14**, 204–220.

8 P. F. Wang, S. H. Shi, J. J. Ma, H. Song, Y. Zhang, C. Gao, C. Z. Zhao, S. Z. Zhao, L. Hou, L. B. Javier, S. J. Fan, F. Xia and X. J. Wang, Global Methylome and gene expression

analysis during early Peanut pod development, *BMC Plant Biol.*, 2018, **18**, 352.

9 C. R. Xie, C. G. You, N. Zhang, H. S. Sheng and X. S. Zheng, Epigallocatechin gallate preferentially inhibits O^6-methylguanine DNA-methyltransferase expression in glioblastoma cells rather than in nontumor glial cells, *Nutr. Cancer*, 2018, **70**, 1339–1347.

10 X. Cheng and R. J. Roberts, AdoMet-dependent methylation, DNA methyltransferases and base flipping, *Nucleic Acids Res.*, 2001, **29**, 3784–3795.

11 D. H. Spencer, D. A. Russler-Germain, S. Ketkar, N. M. Helton, T. L. Lamprecht, R. S. Fulton, C. C. Fronick, M. O'Laughlin, S. E. Heath, M. Shinawi, P. Westervelt, J. E. Payton, L. D. Wartman, J. S. Welch, R. K. Wilson, M. J. Walter, D. C. Link, J. F. DiPersio and T. J. Ley, CpG island hypermethylation mediated by DNMT3A is a consequence of AML progression, *Cell*, 2017, **168**, 801–816.

12 M. Klutstein, D. Nejman, R. Greenfield and H. Cedar, DNA methylation in cancer and aging, *Cancer Res.*, 2016, **76**, 3446–3450.

13 H. Heyn and M. Esteller, DNA methylation profiling in the clinic: applications and challenges, *Nat. Rev. Genet.*, 2012, **13**, 679–692.

14 M. Schapira and C. H. Arrowsmith, Methyltransferase inhibitors for modulation of the epigenome and beyond, *Curr. Opin. Chem. Biol.*, 2016, **33**, 81–87.

15 L. Lennard and H. J. Singleton, High-performance liquid chromatographic assay of human red blood cell thiopurine methyltransferase activity, *J. Chromatogr. B: Biomed. Sci. Appl.*, 1994, **661**, 25–33.

16 I. Reenilä, P. Tuomainen and P. T. Männistö, Improved assay of reaction products to quantitate cate-chol-O-methyltransferase activity by high-performance liquid chromatography with electrochemical detection, *J. Chromatogr. B: Biomed. Sci. Appl.*, 1995, **663**, 137–142.

17 A. Bergerat, W. Guschlbauer and G. V. Fazakerley, Allosteric and catalytic binding of S-adenosylmethionine to escherichia coli DNA adenine methyltransferase monitored by 3H NMR, *Proc. Natl. Acad. Sci. U. S. A.*, 1991, **88**, 6394–6397.

18 M. F. Fraga, E. Uriol, L. B. Diego, M. Berdasco, M. Esteller, M. J. Canal and R. Rodriguez, High-performance capillary elec-trophoretic method for the quantification of 5-methyl 2′-deoxycytidine in genomic DNA: Application to plant, animal and human cancer tissues, *Electrophoresis*, 2018, **23**, 1677–1681.

19 Z. M. Li, X. L. Zhong, S. H. Wen, L. Zhang, R. P. Liang and J. D. Qiu, Colorimetric detection of methyltransferase activity based on the enhancement of CoOOH nanozyme activity by ssDNA, *Sens. Actuators, B*, 2019, **281**, 1073–1079.

20 W. Song, Y. Wang, R. P. Liang, L. Zhang and J. D. Qiu, Label-free fluorescence assay for protein kinase based on pep-tide biomineralized gold nanoclusters as signal sensing probe, *Biosens. Bioelectron.*, 2015, **64**, 234–240.

21 S. Schlücker, Surface-enhanced raman spectroscopy: concepts and chemical applications, *Angew. Chem., Int. Ed.*, 2014, **53**, 4756–4795.

22 L. Guerrini and D. Graham, Molecularly-mediated assemblies of plasmonic nanoparticles for surface-enhanced Raman Spectroscopy applications, *Chem. Soc. Rev.*, 2012, **41**, 7085–7107.

23 M. Moskovits, Persistent misconceptions regarding SERS, *Phys. Chem. Chem. Phys.*, 2013, **15**, 5301–5311.

24 M. G. Albrecht and J. A. Creighton, Anomalously intense Raman spectra of pyridine at a silver electrode, *J. Am. Chem. Soc.*, 1977, **99**, 5215–5217.

25 L. L. Wu, H. B. Pu, L. J. Huang and D. W. Sun, Plasmonic nanoparticles on metal-organic framework: A versatile SERS platform for adsorptive detection of new coccine and orange II dyes in food, *Food Chem.*, 2020, **328**, 127105.

26 Z. S. Wang, Q. Y. Zhu, Y. L. Wang, S. Z. Dou, Q. Y. Chen and N. Lu, Silver-nanoparticle-grafted silicon nanocones for repro-ducible Raman detection of trace contaminants in complex liquid environments, *Spectrochim. Acta, Part A*, 2021, **251**, 119447.

27 Y. J. Zhu, J. F. Wu, K. Wang, H. Xu, M. M. Qu, Z. C. Gao, L. Guo and J. W. Xie, Facile and sensitive measurement of GSH/GSSG in cells by surface-enhanced Raman spectroscopy, *Talanta*, 2020, **224**, 121852.

28 Q. H. He, Y. K. Han, Y. Z. Huang, J. W. Gao, Y. K. Gao, L. Han and Y. Zhang, Reusable dual-enhancement SERS sensor based on graphene and hybrid nanostructures for ultrasensitive lead(II) detection, *Sens. Actuators, B*, 2021, **341**, 130031.

29 R. L. Gieseking, M. A. Ratner and G. C. Schatz, Theoretical modeling of voltage effects and the chemical mechanism in surface-enhanced Raman scattering, *Faraday Discuss.*, 2017, **205**, 149–171.

30 M. Chen, W. Luo, Z. M. Zhang, R. H. Wang, Y. Q. Zhu, H. Yang and X. Q. Chen, Synthesis of Multi-Au-Nanoparticle-Embedded Mesoporous Silica Microspheres as Self-Filtering and Reusable Substrates for SERS Detection, *ACS Appl. Mater. Interfaces*, 2017, **9**, 42156–42166.

31 S. A. Paknejad, G. Dumas, G. West, G. Lewis and S. H. Mannan, Microstructure evolution during 300 degrees C storage of sintered Ag nanoparticles on Ag and Au substrates, *J. Alloys Compd.*, 2014, **617**, 994–1001.

32 M. H. Zhang, G. B. Yi, X. H. Zu, H. L. Huang, Y. J. Wang, J. C. Wang, B. B. Zhong and H. S. Luo, Preparation of Ag Nanowire @ Au Nanoparticle Hybrid Nanowires and their Influence on the Fluorescence Properties of P3HT, *J. Chin. Chem. Soc.*, 2017, **64**, 1308–1315.

33 M. Vinod, R. S. Jayasree and K. G. Gopchandran, Synthesis of pure and biocompatible gold nanoparticles using laser ablation method for SERS and photothermal applications, *Curr. Appl. Phys.*, 2017, **17**, 1430–1438.

34 C. L. Yao, X. N. Gao, X. Liu, Y. H. Shen and A. J. Xie, *In situ* preparation of Ferrero (R) chocolate-like Cu_2O@Ag microsphere as SERS substrate for detection of thiram, *J. Mater. Res. Technol.*, 2021, **11**, 857–865.

35 Y. F. Shan, Y. Yang, Y. Q. Cao, C. L. Fu and Z. R. Huang, Synthesis of wheatear-like ZnO nanoarrays decorated with

Ag nanoparticles and its improved SERS performance through hydrogenation, *Nanotechnology*, 2016, **27**, 145502.

36 N. R. Barveen, T. J. Wang, Y. H. Chang and Z. Yuan-Liu, Ultrasensitive and reusable SERS probe for the detection of synthetic dyes in food industry through hybrid flower-shaped ZnO@Ag nanostructures, *J. Alloys Compd.*, 2021, **861**, 157952.

37 X. Zhao, W. Z. Wang, Y. J. Liang, J. L. Fu, M. Zhu, H. L. Shi, S. J. Lei and C. J. Tao, Visible-light-driven charge transfer to significantly improve surface-enhanced Raman scattering (SERS) activity of self-cleaning TiO_2/Au nanowire arrays as highly sensitive and recyclable SERS sensor, *Sens. Actuators, B*, 2019, **279**, 313–319.

38 X. J. Luo, T. L. Kang, J. T. Zhu, P. Wu and C. X. Cai, Sensitivity-Improved SERS Detection of Methyltransferase Assisted by Plasmonically Engineered Nanoholes Array and Hybridization Chain Reaction, *ACS Sens.*, 2020, **5**, 3639–3648.

39 Y. Li, C. F. Yu, H. X. Han, C. S. Zhao and X. R. Zhang, Sensitive SERS detection of DNA methyltransferase by target triggering primer generation-based multiple signal amplification strategy, *Biosens. Bioelectron.*, 2016, **81**, 111–116.

40 X. M. Wang, M. R. Cui, H. Zhou and S. S. Zhang, DNA-hybrid-gated functional mesoporous silica for sensitive DNA methyltransferase SERS detection, *Chem. Commun.*, 2015, **51**, 13983–13985.

41 X. J. Cui, R. G. Li, X. F. Liu, J. F. Wang, X. Q. Leng, X. L. Song, Q. Q. Pei, Y. Wang, S. Liu and J. D. Huang, Low-background and visual detection of antibiotic based on target-activated colorimetric split peroxidase DNA enzyme coupled with dual nicking enzyme signal amplification, *Anal. Chim. Acta*, 2018, **997**, 1–8.

42 X. W. Xu, L. Wang, W. L. Cui and W. Jiang, An integrated and restructive probe mediated strand displacement amplification strategy for sensitive and specific DNA methyltransferase activity detection, *Sens. Actuators, B*, 2018, **266**, 124–130.

43 J. Ma, L. Wu, Z. H. Li, Z. C. Lu, W. M. Yin, A. X. Nie, F. Ding, B. R. Wang and H. Y. Han, Versatile electrochemilumines-cence assays for PEDV antibody based on rolling circle amplification and Ru-DNA nanotags, *Anal. Chem.*, 2018, **90**, 7415–7421.

44 F. Wang, G. Guo, S. J. Luo and R. B. Guo, H-pi conjugated molecule-based self-assembly of surfactants for promoting me-thane hydrate formation, *ACS Sustainable Chem. Eng.*, 2017, **5**, 1408–1415.

45 H. Chouaibi, B. Rivas-Murias, M. Smari, J. Massoudi, E. Dhahri and V. Salgueirino, Unraveling the multi-featured magnetic behavior of $Nd_{0.75}Sr_{0.25}CoO_3$ perovskite nanocrystals annealed at different temperatures, *J. Alloys Compd.*, 2021, **874**, 159870.

46 S. Khezri, M. Bahram and N. Samadi, A dual-mode nanosensor based on the inner filter effect of gold nanoparticles on the fluorescence of CdS quantum dots for sensitive detection of arginine, *Anal. Methods*, 2017, **9**, 6513–6524.

47 T. Wu, H. Zheng, Y. C. Kou, X. Y. Su, N. R. Kadasala, M. Gao, L. Chen, D. L. Han, Y. Liu and J. H. Yang, Self-sustainable and recyclable ternary Au@Cu2O-Ag nanocomposites: application in ultrasensitive SERS detection and highly efficient photo-catalysis of organic dyes under visible light, *Microsyst. Nanoeng.*, 2021, **7**, 23.

48 K. K. Strelau, A. Brinker, C. Schnee, K. Weber, R. Moller and J. Popp, Detection of PCR products amplified from DNA of epizootic pathogens using magnetic nanoparticles and SERS, *J. Raman Spectrosc.*, 2011, **42**, 243–250.

49 Z. M. Li, Z. H. Zhong, R. P. Liang and J. D. Qiu, The colorimetric assay of DNA methyltransferase activity based on strand displacement amplification, *Sens. Actuators, B*, 2017, **238**, 626–632.

50 J. Zhu, L. Wang, X. Xu, H. Wei and W. Jiang, Modular nuclease-responsive DNA three-way junction-based dynamic as-sembly of a DNA device and its sensing application, *Anal. Chem.*, 2016, **88**, 3817–3825.

51 Y. X. Zhao, F. Chen, Y. Y. Wu, Y. H. Dong and C. H. Fan, Highly sensitive fluorescence assay of DNA methyltransferase ac-tivity via methylation-sensitive cleavage coupled with nicking enzyme-assisted signal amplification, *Biosens. Bioelectron.*, 2013, **42**, 56–61.

52 G. L. Wang, L. Y. Zhou, H. Q. Luo and N. B. Li, Electrochemical strategy for sensing DNA methylation and DNA methyl-transferase activity, *Anal. Chim. Acta*, 2013, **768**, 76–81.

53 R. Z. Chen, H. Y. Shi, X. Y. Meng, Y. Y. Su, H. Y. Wang and Y. He, Dual-amplification strategy-based SERS chip for sensitive and reproducible detection of DNA methyltransferase activity in human serum, *Anal. Chem.*, 2019, **91**, 3597–3603.